

Influence of phenylethylammonium iodide as additive in the formamidinium tin iodide perovskite on interfacial characteristics and charge carrier dynamics

Cite as: APL Mater. 7, 031112 (2019); <https://doi.org/10.1063/1.5083624>

Submitted: 29 November 2018 . Accepted: 27 February 2019 . Published Online: 25 March 2019

Jonas Horn,  Mirko Scholz,  Kawon Oum,  Thomas Lenzer, and  Derck Schlettwein

COLLECTIONS

Paper published as part of the special topic on [Perovskite Semiconductors for Next Generation Optoelectronic Applications](#)



View Online



Export Citation



CrossMark

ARTICLES YOU MAY BE INTERESTED IN

[Effects of strontium doping on the morphological, structural, and photophysical properties of FASnI₃ perovskite thin films](#)

APL Materials **7**, 031116 (2019); <https://doi.org/10.1063/1.5087110>

[Unusual defect physics in CH₃NH₃PbI₃ perovskite solar cell absorber](#)

Applied Physics Letters **104**, 063903 (2014); <https://doi.org/10.1063/1.4864778>

[Temperature-dependent studies of exciton binding energy and phase-transition suppression in \(Cs,FA,MA\)Pb\(I,Br\)₃ perovskites](#)

APL Materials **7**, 031113 (2019); <https://doi.org/10.1063/1.5083792>



Influence of phenylethylammonium iodide as additive in the formamidinium tin iodide perovskite on interfacial characteristics and charge carrier dynamics

Cite as: APL Mater. 7, 031112 (2019); doi: 10.1063/1.5083624
Submitted: 29 November 2018 • Accepted: 27 February 2019 •
Published Online: 25 March 2019



View Online



Export Citation



CrossMark

Jonas Horn,¹ Mirko Scholz,²  Kawon Oum,^{2,a)}  Thomas Lenzer,^{2,a)}  and Derck Schlettwein^{1,a)} 

AFFILIATIONS

¹Institute of Applied Physics, Justus Liebig University Giessen, Heinrich-Buff-Ring 16, 35392 Giessen, Germany

²Physical Chemistry, University of Siegen, Adolf-Reichwein-Str. 2, 57076 Siegen, Germany

Note: This paper is part of the special topic on Perovskite Semiconductors for Next Generation Optoelectronic Applications.

^{a)}Electronic addresses: oum@chemie.uni-siegen.de; lenzer@chemie.uni-siegen.de; and schlettwein@uni-giessen.de.

ABSTRACT

A combined electrical and time-resolved optical investigation of the perovskite formamidinium tin iodide (FASnI₃) and its phenylethylammonium (PEA) derivative PEA_{0.08}FA_{0.92}SnI₃, which recently achieved a power conversion efficiency of 9%, is presented to study the specifics of contact characteristics and charge carrier dynamics. Microstructured gold electrode arrays were used to investigate the charge transport across a metal-perovskite interface and through micrometers of the perovskite films. Symmetrical contact configuration enabled detailed polarization studies. Hysteresis in the current-voltage characteristics and a corresponding current-time behavior indicated limitations by charge transfer in the contacts. Hysteresis was less pronounced in PEA_{0.08}FA_{0.92}SnI₃ compared with FASnI₃. This is explained by a 2-dimensional interlayer at the contacts, which leads to decreased field-induced migration of ions at the contact. Carrier recombination in the bulk of FASnI₃ films, however, was only slightly modified by the presence of PEA. Femtosecond broadband transient absorption experiments up to 1.5 ns provided rate constants for the Auger and bimolecular recombination processes in FASnI₃ of $k_3 = 1 \times 10^{-29} \text{ cm}^6 \text{ s}^{-1}$ and $k_2 = 3.1 \times 10^{-10} \text{ cm}^3 \text{ s}^{-1}$, respectively. In PEA_{0.08}FA_{0.92}SnI₃, no significant differences in k_2 and an only slightly increased $k_3 = 2 \times 10^{-29} \text{ cm}^6 \text{ s}^{-1}$ were measured. In extension to previous photoluminescence studies, we found efficient cooling of hot carriers by coupling to optical phonons ($\tau_{\text{cop}} = 0.5 \text{ ps}$), which is even faster than in lead perovskites.

© 2019 Author(s). All article content, except where otherwise noted, is licensed under a Creative Commons Attribution (CC BY) license (<http://creativecommons.org/licenses/by/4.0/>). <https://doi.org/10.1063/1.5083624>

During the last decade, organic-inorganic perovskites have attracted a lot of scientific interest due to their semiconductor properties, qualifying them for prospective applications in electronics and optoelectronics, most importantly in thin film photovoltaic devices. Despite power conversion efficiencies (PCEs) exceeding 23%,¹ several aspects remain challenging: the interfaces of the perovskite layer to the adjacent hole- and electron-collecting layers play a major role in device degradation,² which are one of the limiting factors in device performance and can often be detected by hysteresis in the current-voltage characteristics.³ Furthermore, state-of-the-art perovskite solar cells contain lead as the divalent metal ion that raises serious concern because of its toxicity and

the water solubility of lead salts as decomposition products of the perovskite layers. Therefore, substitution of lead is an important task, with tin being one of the most promising candidates.⁴ Formamidinium tin iodide (FASnI₃) has been used successfully as an absorbing layer in solar cells⁵⁻⁸ and has, further, shown promising optical and electronic properties, such as a direct bandgap, a low exciton binding energy, hot-carrier photoluminescence (PL),⁹ and a high charge-carrier mobility.¹⁰ Tin-based perovskites, however, are prone to oxidation of Sn(II) to Sn(IV), generating a high majority charge carrier concentration and, thus, increased recombination rates of light-induced minority carriers and even significantly decreased shunt resistances caused by metallic characteristics of the

perovskite layer.^{11,12} To overcome this problem, several additives in film preparation have been used starting with SnF_2 ,⁵ which has been successfully employed in most FASnI_3 -based solar cells reported so far to reduce the background charge carrier density. Overstoichiometric amounts of tin, which can also be provided through other tin sources, play a crucial role to suppress the formation of Sn(IV) .^{13,14} A further successful approach to yield stabilized Sn(II) -perovskites consists in partial replacement of FA by larger cations, such as butylammonium or phenylethylammonium (PEA), to induce the growth of mixed 2D/3D perovskite layers,^{15–18} a strategy successfully used previously for lead-based perovskites.^{19–21} So far, this approach has resulted in one of the highest PCEs reported for a FASnI_3 -based device of up to 9% through replacement of 8% of the FA by bulkier PEA cations ($\text{PEA}_{0.08}\text{FA}_{0.92}\text{SnI}_3$).¹⁶

In this work, we use a combination of electrical and optical methods to investigate the impact of FA/PEA-exchange on the optoelectronic properties of FASnI_3 . Using microstructured gold arrays, we characterized thin films of FASnI_3 with and without small amounts of phenylethylammonium iodide (PEAI) to investigate their electronic properties. The role of the 2D-interlayer in contact formation is studied, and the relevance of barriers for charge injection is investigated. Ionic migration and its connection with observed hysteresis phenomena are discussed. We employ steady-state absorption and PL measurements as well as ultrafast transient broadband absorption experiments to understand the charge recombination and carrier cooling processes in FASnI_3 and $\text{PEA}_{0.08}\text{FA}_{0.92}\text{SnI}_3$ perovskite layers upon photoexcitation and to differentiate between an influence of PEA on either bulk or interface properties.

Interdigitated microelectrodes with a gap width of 40 μm were prepared via photolithography onto highly n-doped silicon wafers with a thermally grown oxide layer of 300 nm, as described previously.²² 50 nm of gold was deposited as a metal electrode by thermal evaporation. The samples for optical characterization were prepared on soda lime glass (Carl Roth) that was cleaned with RBS solution (Carl Roth), acetone, and *n*-propanol in an ultrasonic bath for 15 min, subsequently.

Prior to the deposition of the perovskite layer, the substrates were treated in a UV/ozone atmosphere for 10 min and then directly transferred into a nitrogen-filled glovebox (<1 ppm O_2 , <1 ppm H_2O). The perovskite deposition was adopted from Ref. 16. For the FASnI_3 films, 172 mg formamidinium iodide (FAI, Greatcell Solar), 372.5 mg SnI_2 (own synthesis according to Ref. 23 with subsequent purification by sublimation), and 15.6 mg SnF_2 (Sigma Aldrich, 99%) were mixed by stirring in 800 μl *N,N*-dimethylformamide (DMF, Alfa Aesar) and 200 μl dimethyl sulfoxide (DMSO, Alfa Aesar), resulting in a bright yellow solution. For the mixed 2D/3D-perovskite films, the amount of FAI was reduced to 158.2 mg and substituted by 19.9 mg PEA (Sigma Aldrich, 99%), resulting in a molar ratio of 0.92:0.08. The concentration of the precursor solutions was reduced from 1M for layers prepared on microstructured arrays to 0.25M for the layers used for optical transmission measurements to reduce film thickness, resulting in a desired lower optical density. The perovskite layer was deposited via spin-coating for 60 s at 4000 rpm onto the microstructured metal electrode arrays or at 8000 rpm onto the glass slides. During the spin-coating, 200 μl of the antisolvent toluene (Alfa Aesar) were dripped onto the substrate. Directly after spin-coating, the layers were annealed at 65 °C for

20 min. The preparation resulted in a thickness of around 450 nm for layers prepared on the metal electrode arrays and 250 nm for layers on glass, as measured by SEM.

The electrical characterization was carried out under dark conditions inside the inert glovebox atmosphere at room temperature using an *IviumStat* potentiostat. Unless stated otherwise, the *j*-*V* measurements were done at a scan rate of 200 mV s⁻¹. Since we found that the current is limited by a barrier at the interfaces, the measured currents were divided by the respective electrode area to yield current densities. A Zeiss Merlin HREM was used for the SEM characterization. X-ray diffractometry was carried out with Cu-K α irradiation using a Siemens D5000 in Bragg-Brentano geometry or a PANalytical X'Pert PRO for grazing incidence.

Femtosecond Vis-NIR broadband transient absorption spectra were obtained using a previously described setup²⁴ employing the pump-supercontinuum probe (PSCP) method.²⁵ Thin films were mounted inside a nitrogen-flushed aluminum cell,²⁶ which was constantly moved during the experiments to expose a fresh sample spot for every pump-probe cycle. The perovskite sample was pumped at 390 nm and probed in transmission geometry over the wavelength range 500–920 nm (cross-correlation ca. 80 fs). The angle between the pump and probe beams was ca. 10°, and the beams were polarized at the magic angle. A calibrated CCD camera was employed to control the pump beam diameter at the sample. The energy of the pump pulse was measured by a calibrated photodiode. The laser fluence was 209 $\mu\text{J cm}^{-2}$, resulting in an initial carrier density of $1.4 \times 10^{20} \text{ cm}^{-3}$. Steady-state absorption spectra of the thin films were recorded on a Varian Cary 5000 double-beam spectrophotometer. Photoluminescence was measured under steady-state conditions following excitation at about 45° with a Nitride NS355L5RLO UV-LED (360 nm) and detection perpendicular to the surface with a TEC5 MultiSpec SC-MCS CCD UV-NIR diode array spectrometer.

Importantly, all steps of the preparation, analysis (except for XRD and SEM), and spectroscopic investigation of the tin perovskite samples were carried out in an inert atmosphere of dry nitrogen, including the use of nitrogen-filled transfer chambers and cells. Samples were stored in the dark, when not in use. This way, decomposition reactions of the tin perovskites were minimized.

Independent of the addition of PEA, the films exhibited a homogeneous coverage of the substrates. This was explicitly shown for the films across the metal electrodes and insulating SiO_2 gaps of the microstructured electrode arrays by SEM in top view (Figs. S1 and S2), or, even more characteristically, in the cross-section (Fig. S3). The size of the crystalline domains showed a fairly uniform appearance, independent of the substrate but systematically differing dependent on the addition of PEA, which led to more extended crystalline domains with, however, some smaller crystals remaining. Aside from a small number of pinholes in case of the $\text{PEA}_{0.08}\text{FA}_{0.92}\text{SnI}_3$ layer, the morphology and size of crystalline domains of all measured perovskite thin films are almost identical to those reported in the literature for FASnI_3 as well as for $\text{PEA}_{0.08}\text{FA}_{0.92}\text{SnI}_3$.¹⁶

For all the films, the X-ray diffraction patterns (Fig. S4) were consistent with the expected orthorhombic structure of FASnI_3 . Comparing the intensity *I* of the (100)-reflex at 14.05° with that of the (120)-reflex at 24.4° yields a ratio of $I_{(100)}/I_{(120)} = 5.05$ for $\text{PEA}_{0.08}\text{FA}_{0.92}\text{SnI}_3$ and $I_{(100)}/I_{(120)} = 2.33$ for FASnI_3 . Compared with

$I_{(100)}/I_{(120)} = 2.56$ reported for single crystals of FASnI_3 ,²³ these results indicate almost random relative positioning of FASnI_3 crystals in our films as opposed to a preferential crystal growth in (100)-direction for $\text{PEA}_{0.08}\text{FA}_{0.92}\text{SnI}_3$ films. This highly ordered structure is expected to reduce the defect formation and is therefore beneficial for a reduced charge carrier concentration and improved PCEs.¹⁶ The $\text{PEA}_{0.08}\text{FA}_{0.92}\text{SnI}_3$ films showed an additional reflex at $2\theta = 3.8^\circ$, confirming the presence of the two-dimensional layered perovskite phase consisting of alternating bilayers of phenylethylammonium ions and bilayers of SnI_6 octahedra, as reported earlier.^{15,16} In diffractograms collected at grazing incidence (Fig. S5), it is confirmed that the layered perovskite is exclusively formed close to the interface with the substrate since the signal at $2\theta = 3.8^\circ$ disappears for angles smaller than 0.5° between the incoming X-ray and the substrate surface.^{15,16}

The electrical measurements provide insights regarding charge carrier transport and ion migration especially at the interfaces, characterizing the specifics of FASnI_3 and, in particular, the influence of PEA. In Fig. 1, the j - V -characteristics of either FASnI_3 films or $\text{PEA}_{0.08}\text{FA}_{0.92}\text{SnI}_3$ films contacted by gold microelectrodes are compared in the range of ± 1 V. For increasing bias starting from 0 V, in the case of FASnI_3 (black squares), we at first observe a small increase of the current (1) which gradually increases for higher bias (2). Upon scan reversal, a further increase of the current was observed despite decreasing bias voltage (3) before the current decreased back to 0 mA cm^{-2} at zero bias (4). The current density, therefore, was significantly larger on this back-sweep. We assign these characteristics to a continuously decreasing resistance for charge transfer R_{CT} at the perovskite/metal interface with increasing bias voltage similar to the diode characteristics, as discussed earlier in similar experiments on MAPbI_3 ,^{27,28} but with significantly larger extent of hysteresis for the present experiments on FASnI_3 . Due to the symmetrical device geometry, identical characteristics were observed in the negative bias direction aside from slightly smaller currents as discussed later.

Hysteresis phenomena are well known from lead-based^{29,30} and tin-based¹⁷ perovskite solar cells and are usually divided into regular (decreased current in forward direction) and inverted (decreased current in reverse direction) hysteresis.³¹ The former was explained by a persistent polarization^{32,33} or the presence of defects in the perovskite film.³⁴ The latter was attributed to a chemical modification of the interface³⁵ or a change of the barrier height at the perovskite-metal junction.^{27,28} What we observe here is the equivalent to the inverted hysteresis in solar cells. Noma *et al.*

recently observed similar I - V characteristics for MASnI_3 films in the positive bias range. They explained a decreased current by trap-filling followed by an increased current when traps were filled. Under negative bias, however, the current was reduced upon scan reversal, which they explained by a recombination of injected carriers with already trapped carriers of different sign which was incompatible with ionic migration and trap-filling by mobile ions.³⁶ Since we, in contrast, observe symmetric hysteresis, we assign the observed current increase upon scanning and continued beyond each scan reversal to a decrease of R_{CT} caused by a decreased injection barrier as a consequence of ion migration at increased applied electric fields.^{27,28} Iodine vacancies which were explicitly found to be the most mobile species in MAPbI_3 ³⁷ and which have also been calculated to be present in FASnI_3 ³⁸ aside from Sn vacancies and interstitial FA are the most likely ionic species to cause such decreased injection barrier.

An increased scan rate [Fig. 1(b)] led to similar characteristics of FASnI_3 with, however, smaller current densities, and a smaller extent of hysteresis pointing at a slow change of R_{CT} relative to the scan rate. The change of R_{CT} with time was directly monitored by measuring the current density at a fixed bias voltage of 1 V [Fig. 2(a)]. Two characteristic time regimes were observed: a fast increase within seconds and a subsequent slower increase. The current density increased to 7 mA cm^{-2} after 100 s, far beyond the 1.5 mA cm^{-2} , e.g., observed in Fig. 1(a) at 200 mV s^{-1} . Even after 100 s, a steady-state was not reached. This is fully consistent with the current increase upon scan reversal in Fig. 1(a), where continued polarization led to a further increase of the current as well. The j - V curves of FASnI_3 following such prolonged polarization [Fig. 2(b)] showed characteristic differences to those measured before [Fig. 1(a)]. Interestingly, the scan towards positive bias showed slightly enhanced current densities at widely preserved shape of the curve. Obviously, the strongly increased j following prolonged polarization [Fig. 2(a)] quickly decreased back to almost the original value within about tens of seconds at 0 V upon the start of the j - V cycle. The second cycle into the positive direction almost resembled the original curve in Fig. 1(a), speaking in favor of a fully recovered R_{CT} indicative of a rapid dissipation of the accumulated iodide vacancies. During the following 40 cycles (Fig. S6), this recovery was completed. In the negative scan direction, however, quite persistently, a strongly decreased current density was observed. During the prolonged positive polarization, a persistent barrier for charge injection in the other (negative) direction evolved. Such

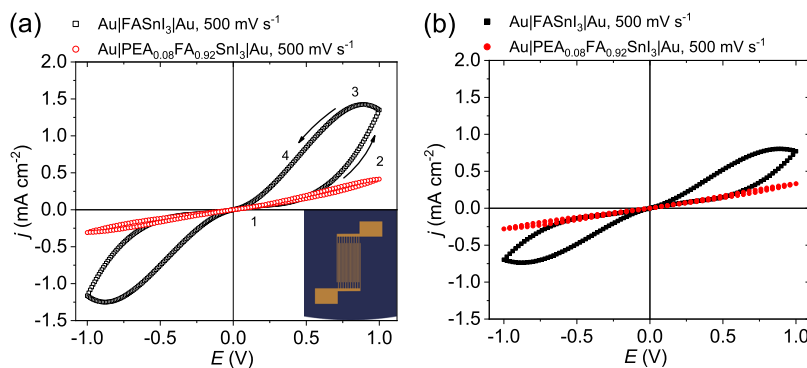


FIG. 1. (a) j - V -characteristics of thin films of FASnI_3 (black) and $\text{PEA}_{0.08}\text{FA}_{0.92}\text{SnI}_3$ (red) prepared on interdigitated gold μ -structures (see inset). (b) j - V characteristics obtained with a scan rate of 500 mV s^{-1} .

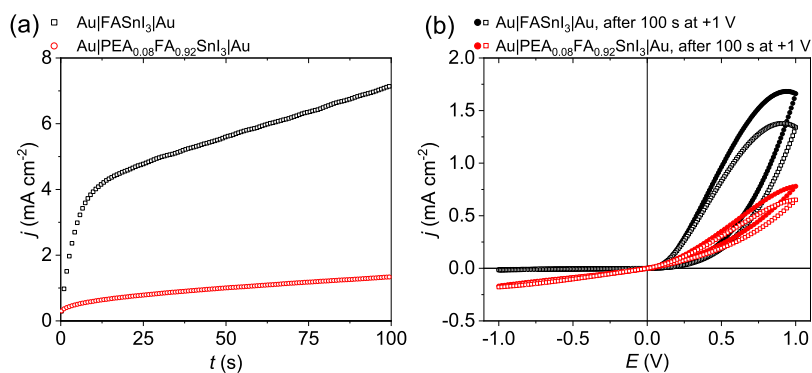


FIG. 2. (a) Current density for FASnI₃ (black) and PEA_{0.08}FA_{0.92}SnI₃ (red) films while applying a bias of 1 V. (b) j - V characteristics after applying a bias of 1 V for 100 s. Open and filled symbols represent the first and second measurement cycle, respectively.

persistence is reminiscent of the changes supposedly caused by slowly moving ions observed, e.g., for MAPbI₃ at lower temperatures.²⁷ For FASnI₃, it has been calculated that Sn vacancies represent the defect with lowest formation energy and, hence, highest concentration. For MAPbI₃, a low mobility of lead vacancies has been reported.³⁷ Our present results would be well explained by slowly moving tin vacancies, which would accumulate during prolonged polarization at the negative electrode, leading to blocking characteristics similar to a diode in reverse direction. This accumulation is persistent over several measurement cycles (see Fig. S6), as shown by the minimal recovery of the original j - V characteristics after ten measurements and still only partial recovery even after 40 cycles following dissipation of the accumulated tin vacancies.

The partial substitution of FAI by PEAI influences the j - V characteristics substantially, as shown in Fig. 1(a). First, the current for PEA_{0.08}FA_{0.92}SnI₃ was smaller than for FASnI₃ by a factor of four. This can be explained either by a lower defect density and, thus, reduced charge carrier density for PEA_{0.08}FA_{0.92}SnI₃, by a lower charge carrier mobility caused by blocking of charge carriers at the 2D perovskite interlayers, or by screening of the electric field induced by the 2D interlayer. Since a slightly smaller relative dielectric constant has been calculated³⁹ for the two-dimensional perovskites, the latter can be ruled out. Second, the current for PEA_{0.08}FA_{0.92}SnI₃ increased almost linearly with the voltage opposed to the increasing slope observed for FASnI₃. This speaks in favor of an ohmic contact rather than a blocking contact and, hence, a sufficiently small and constant R_{CT} . Compatible with this finding, PEA_{0.08}FA_{0.92}SnI₃ showed a considerably reduced hysteresis which points at a smaller change in R_{CT} as a result of the applied bias. By comparing the current density for the bias sweep back and forth at 0.5 V, we see an increase by a factor of 1.3 in comparison with a factor of five for pure FASnI₃. As shown by grazing-incidence XRD measurements (Fig. S5), the 2D perovskite layer is located directly at the substrate. Such interlayer can be assumed to attenuate ion migration and thereby reduce the influence of mobile ions at the electrode surface, leading to the strong suppression of hysteresis. Chen *et al.* similarly reported a reduced hysteresis resulting from PEABr in FASnI₃-based solar cells which was explained by such passivation of traps at the interface.¹⁷ Furthermore, an increased scan rate [Fig. 1(b)] showed an only minor influence on the j - V curve, confirming such ohmic characteristics at widely preserved current and a reduced influence of migrating ions relative to FASnI₃.

Despite the small influence of ion migration on the electrical characteristics of PEA_{0.08}FA_{0.92}SnI₃ observed during cycling, a significant influence could be enforced during [Fig. 2(a)] and following [Fig. 2(b)] prolonged polarization. A steadily increasing current was observed while applying a constant bias indicating slightly decreasing R_{CT} caused by ionic movement under these conditions, albeit to significantly less extent than found for FASnI₃ [Fig. 2(a)]. The qualitative change of the j - V characteristics found for PEA_{0.08}FA_{0.92}SnI₃ after such prolonged polarization was similar to that found for FASnI₃ [Fig. 2(b)]. However, for positive bias voltages, the current was increased, e.g., by a factor of 1.9 at 1 V as opposed to a factor of 1.2 for FASnI₃, consistent with a slightly but persistently reduced R_{CT} . Furthermore, under negative bias, about 60% of the current before prolonged polarization were still measured for PEA_{0.08}FA_{0.92}SnI₃ as opposed to the blocking characteristics of FASnI₃ with only about 1% of the current left. This suggests a less pronounced or even absent barrier for charge transport in the negative direction in the case of PEA_{0.08}FA_{0.92}SnI₃. This is fully consistent with a reduced influence of ionic migration and further indicates that the influence of ions modifying the injection barriers despite the two-dimensional interlayer is more persistent (Fig. S7).

In addition to the electric analysis, the two thin-film materials were investigated by steady-state optical methods and ultrafast transient absorption spectroscopy, which sensitively probe properties of the charge carriers across the whole film thickness. Figure 3(a) shows steady-state absorption and PL spectra of FASnI₃ and PEA_{0.08}FA_{0.92}SnI₃. Except for a minor difference in the absolute optical density of both samples, the absorption spectra look very similar. In both cases, the band edge is located at 870 nm (1.43 eV, determined from the zero-crossing of the second derivative). This is in very good agreement with the previous results from spectroscopic ellipsometry.⁴⁰ The corresponding PL emission peak appears close to the band edge: 881 nm (1.407 eV, FWHM 104 meV) for FASnI₃ and 878 nm (1.413 eV, FWHM 103 meV) for PEA_{0.08}FA_{0.92}SnI₃. The measured width of the PL bands is consistent with the emission of a thermal carrier distribution at 300 K. The weak blue-shift upon PEA addition agrees well with the results of a previous study by Liao *et al.*¹⁵ and may be taken as an indication for an increased confinement of the charge carriers due to the influence of lower-dimensional tin perovskite domains. The results of Liao *et al.* and our results are therefore at variance with the study of Shao *et al.* who observed a systematic red-shift of the PL upon PEA addition, which is in contrast to expectations, e.g., 891 nm (1.391 eV, FWHM

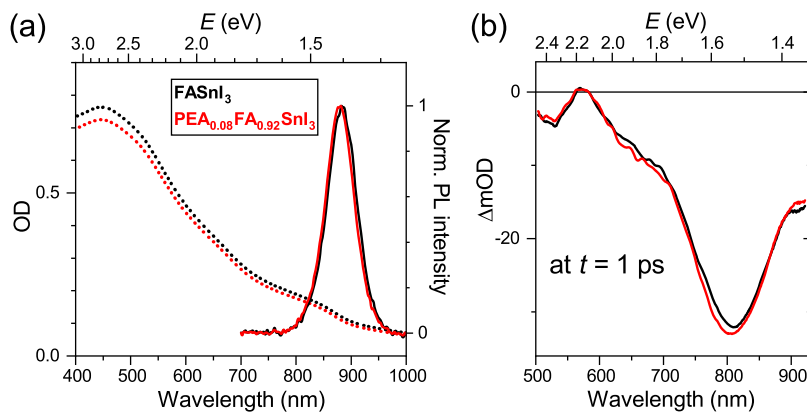


FIG. 3. (a) Steady-state absorption (dotted lines) and normalized photoluminescence spectra (solid lines, $\lambda_{\text{exc}} = 360$ nm) for FASnI_3 (black) and $\text{PEA}_{0.08}\text{FA}_{0.92}\text{SnI}_3$ (red) thin films. (b) Corresponding transient absorption spectra at a delay time of 1 ps after photoexcitation at 390 nm.

96 meV) for FASnI_3 and 896 nm (1.383 eV, FWHM 95 meV) for $\text{PEA}_{0.08}\text{FA}_{0.92}\text{SnI}_3$.¹⁶ The reason for this deviation is currently unclear. We also note that we did not find any indication for a separate emission band of a 2D perovskite phase at shorter wavelengths. This is in agreement with the previous observations of Liao *et al.*, who did not observe such low-wavelength PL either, even for $\text{PEA}_{0.20}\text{FA}_{0.80}\text{SnI}_3$.¹⁵

Figure 3(b) shows a comparison of transient absorption spectra for both samples at a fixed time delay of 1 ps after photoexcitation. We note that, aside from a small spectral blue-shift for the $\text{PEA}_{0.08}\text{FA}_{0.92}\text{SnI}_3$ sample, the pronounced bleach band around 800 nm and even very small spectral features, such as the weak absorption at about 570 nm, exhibit only minor differences for the two samples. It is thereby confirmed that the observed changes in the

electric properties by substitution of FAI by PEAI are mainly caused by modification of interfacial rather than bulk properties.

A detailed comparison of the transient absorption spectra for both compounds is provided in Fig. 4. Around zero time delay [panels (a) and (e)], we observe a pronounced bleach feature centered at 530 nm, which is due to the depletion of carriers in the valence band (VB). The bleach is accompanied by substantial absorption above 820 nm, which arises from band-gap renormalization. We note that a similar absorption feature has been previously observed for lead perovskites, such as MAPbI_3 , and assigned to the same process.^{41,42}

In panels (b) and (f), we observe the spectral development up to 1.5 ps. The bleach feature shows an ultrafast shift toward the band edge, and at the same time, the band-gap renormalization feature disappears. A global kinetic analysis of the complete set of

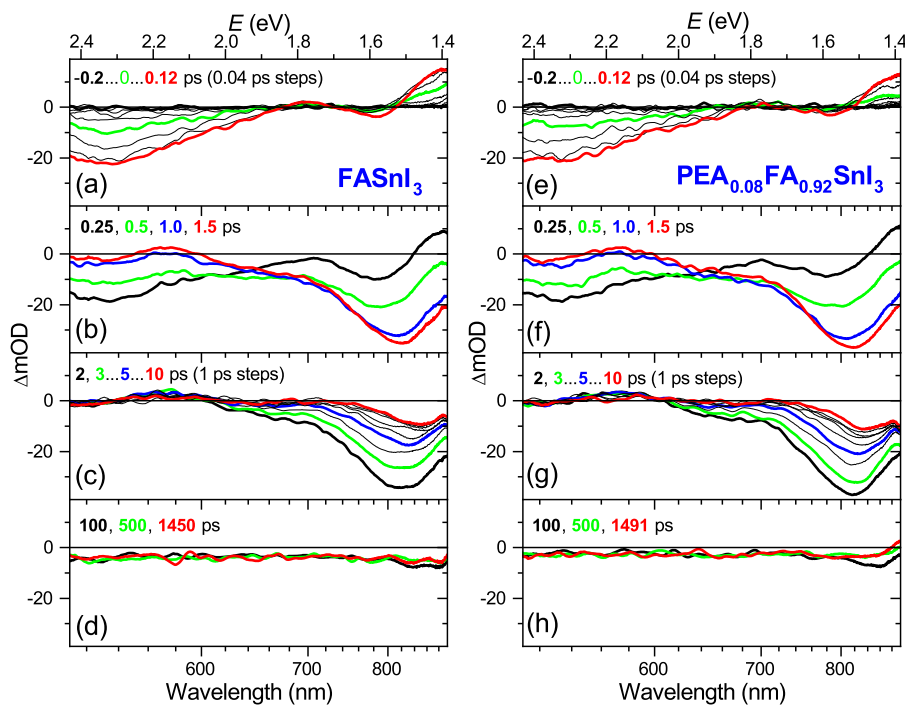


FIG. 4. Broadband transient absorption spectra for FASnI_3 [panels (a)–(d)] and $\text{PEA}_{0.08}\text{FA}_{0.92}\text{SnI}_3$ [panels (e)–(h)] upon excitation at 390 nm. The different panels from top to bottom indicate the different time ranges of interest.

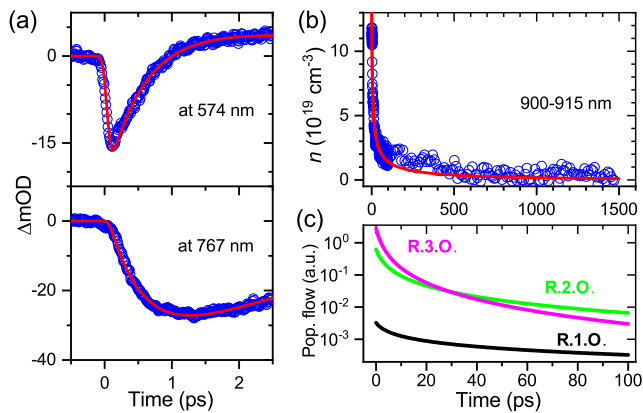


FIG. 5. (a) Kinetic traces for FASnI₃ probed at 574 and 767 nm upon excitation at 390 nm including fit results from a global kinetic analysis (red lines). (b) Decay of charge carrier density due to recombination as monitored in the NIR region (900–915 nm) including a fit based on the recombination model described in the text. (c) Population flow obtained from the kinetic analysis indicating the relative importance of third-order (R.3.O.), second-order (R.2.O.), and first-order (R.1.O.) contributions at different time ranges.

transient spectra provides a time constant $\tau_{\text{cop}} = 0.5$ ps for this process, as shown in Fig. 5(a) for two representative kinetics at 574 and 767 nm. The type of spectral change and the associated time scale strongly suggest that it is associated with the fast relaxation of “hot” charge carriers toward the band edge due to efficient carrier–optical phonon scattering, dissipating more than 1 eV of excess energy. The time constant is smaller than for MAPbI₃.^{41,42} In the latter case, τ_{cop} varies, e.g., between 0.9 and 2.8 ps over the carrier density range 5.0×10^{17} to 1.3×10^{19} cm⁻³, indicating a “phonon bottleneck” for carrier cooling. A similar situation was encountered in the case of FAPbI₃.⁴³ Such an effect is obviously not present for the FASnI₃ compounds studied here although the initial carrier density is even slightly larger (1.4×10^{20} cm⁻³). The transient absorption results, therefore, show that hot carriers probed by our sub-ps experiments (starting from 900 meV excess energy above the band edge) are cooled significantly faster than those probed in a range of 150–75 meV excess energy by changes of an asymmetric PL emission band of FASnI₃ observed at higher pump fluence in the nanosecond regime.⁹

In panels (c) and (g), covering the time scale up to 10 ps, we observe a substantial decay of the bleach band. This must be due to the fastest part of charge carrier recombination. Even on longer time scales up to 1500 ps [panels (d) and (h)], the recombination apparently slows down strongly. To characterize the electron-hole recombination in more detail, the decay of the bleach feature was analyzed by a kinetic model involving processes of third order (Auger-type, rate constant k_3), second order (radiative bimolecular, k_2), and first order (trap-assisted Shockley-Read-Hall, k_1). The rate constant $k_1 = 2.3 \times 10^8$ s⁻¹ (corresponding to $\tau_1 = 4.32$ ns) for FASnI₃ was taken from the literature¹⁶ because the time range covered in the current study was limited to 1.5 ns. The initial charge carrier density of 1.4×10^{20} cm⁻³ was determined using the measured fluence of the pump beam ($209 \mu\text{J cm}^{-2}$) and the known absorption coefficient and reflectivity of FASnI₃ at 390 nm.⁴⁰

The resulting best fit is shown in Fig. 5(b) and it provides values of $k_3 = 1 \times 10^{-29}$ cm⁶ s⁻¹ and $k_2 = 3.1 \times 10^{-10}$ cm³ s⁻¹. Both rate constants agree well with the results from THz measurements by Milot *et al.* ($k_3 = 9.3 \times 10^{-30}$ cm⁶ s⁻¹ and $k_2 = 2.3 \times 10^{-10}$ cm³ s⁻¹).¹⁰

Contributions to the “population flow” during carrier recombination are analyzed in Fig. 5(c). The analysis shows that the fast decay of the bleach band over the first 25 ps is governed by Auger recombination, whereas radiative electron-hole recombination becomes more important afterwards. Up to 100 ps, trap-state-mediated monomolecular recombination plays no role and only becomes important on much longer time scales. An analogous analysis for the charge carrier recombination in PEA_{0.08}FA_{0.92}SnI₃ (with k_1 fixed at 1.6×10^8 s⁻¹, corresponding to $\tau_1 = 6.29$ ns)¹⁶ yields the same value for the rate constant k_2 , only the rate constant k_3 is slightly elevated ($k_3 = 2 \times 10^{-29}$ cm⁶ s⁻¹). This suggests a small influence of the PEA additive on both recombination processes. We note that the rate constants k_2 and k_3 are substantially lower than in lead perovskites, confirming the potential of tin perovskite compounds with respect to optoelectronic applications.⁴⁴ They are also lower than in the MASnI₃ perovskite.⁴⁵ A previous study found a small decrease of the rate constant k_1 from 2.3×10^8 s⁻¹ to 1.6×10^8 s⁻¹, suggesting slightly reduced trap-assisted nonradiative recombination upon partial exchange of FA by PEA.¹⁶ The only small change in k_1 is also supported by similar PL intensities we have found for FASnI₃ and PEA_{0.08}FA_{0.92}SnI₃. As a result, both compounds exhibit similar properties regarding charge carrier recombination.

Concluding the above, in the steady-state and transient optical experiments, we find an only weak influence of the exchange of 8% FA by PEA on the carrier–optical phonon scattering time constant and the recombination rate constants of the FASnI₃ perovskite. Our transient absorption results clearly show fast relaxation of hot carriers in FASnI₃ and PEA_{0.08}FA_{0.92}SnI₃, dissipating a large amount of the 900 meV excess energy (above band edge) into the lattice within 0.5 ps. This finding significantly extends previous observations, based on PL experiments, which found dissipation of 75–150 meV within a few ns.⁹ The related claim that this material might be well suited for hot-carrier extraction would then apply to the range of small carrier excess energies only. PEA does not significantly change the electronic bulk properties of the material, but mainly brings structural improvements to the FASnI₃ perovskite, in particular, by the formation of a two-dimensional interlayer at the substrate. A specific role of such interlayers in electronic contact formation was detected in conductance measurements on PEA_{0.08}FA_{0.92}SnI₃ compared with FASnI₃. A detailed analysis of the *j*-*V* characteristics measured for FASnI₃ on microstructured electrode arrays revealed significant hysteresis caused by changes in the interfacial charge-transfer resistance, presumably as a result of ion migration in applied electric fields. Two different effects in the positive or negative transport direction after positive prolonged polarization and two different time scales of relaxation of the corresponding barriers indicate migration of two ionic species, namely, iodine and tin vacancies. Partial substitution of FA by PEA influences the injection characteristics at the metal-perovskite interface substantially. The effect of migrating ions is reduced, but the change of the interface is more persistent due to a better stabilization in the 2D interlayer at the contact.

See [supplementary material](#) for SEM and XRD characterization of the films and additional j - V characteristics.

The authors thank the Deutsche Forschungsgemeinschaft (DFG) for financial support (Nos. SCHL 340/21-3, OU 58/10-3, LE 926/11-3, and RTG 2204). We are also grateful to R. Kentsch for complementary steady-state absorption and PL measurements, M. Morgenroth for assistance during the transient absorption experiments, H. Hemmelmann for measuring XRD at grazing incidence, and ZfM/LaMa (JLU Gießen) for support in SEM and photolithography.

REFERENCES

- ¹National Renewable Energy Laboratory, U.S. Department of Energy, Efficiency Chart, 2018, <https://www.nrel.gov/pv/assets/pdfs/pv-efficiencies-07-17-2018.pdf>.
- ²J. A. Christians, P. Schulz, J. S. Tinkham, T. H. Schloemer, S. P. Harvey, B. J. Tremolet de Villers, A. Sellinger, J. J. Berry, and J. M. Luther, *Nat. Energy* **3**, 68 (2018).
- ³A. Fakharuddin, L. Schmidt-Mende, G. Garcia-Belmonte, R. Jose, and I. Mora-Sero, *Adv. Energy Mater.* **7**, 1700623 (2017).
- ⁴A. Abate, *Joule* **1**, 659 (2017).
- ⁵T. M. Koh, T. Krishnamoorthy, N. Yantara, C. Shi, W. L. Leong, P. P. Boix, A. C. Grimsdale, S. G. Mhaisalkar, and N. Mathews, *J. Mater. Chem. A* **3**, 14996 (2015).
- ⁶W. Liao, D. Zhao, Y. Yu, C. R. Grice, C. Wang, A. J. Cimaroli, P. Schulz, W. Meng, K. Zhu, R.-G. Xiong, and Y. Yan, *Adv. Mater.* **28**, 9333 (2016).
- ⁷Z. Zhu, C.-C. Chueh, N. Li, C. Mao, and A. K.-Y. Jen, *Adv. Mater.* **30**, 1703800 (2017).
- ⁸J. Xi, Z. Wu, B. Jiao, H. Dong, C. Ran, C. Piao, T. Lei, T.-B. Song, W. Ke, T. Yokoyama, X. Hou, and M. G. Kanatzidis, *Adv. Mater.* **29**, 1606964 (2017).
- ⁹H.-H. Fang, S. Adjokatse, S. Shao, J. Even, and M. A. Loi, *Nat. Commun.* **9**, 151 (2018).
- ¹⁰R. L. Milot, G. E. Eperon, T. Green, H. J. Snaith, M. B. Johnston, and L. M. Herz, *J. Phys. Chem. Lett.* **7**, 4178 (2016).
- ¹¹D. B. Mitzi, C. A. Feild, W. T. A. Harrison, and A. M. Guloy, *Nature* **369**, 467 (1994).
- ¹²F. Hao, C. C. Stoumpos, D. H. Cao, R. P. H. Chang, and M. G. Kanatzidis, *Nat. Photonics* **8**, 489 (2014).
- ¹³S. J. Lee, S. S. Shin, J. Im, T. K. Ahn, J. H. Noh, N. J. Jeon, S. I. Seok, and J. Seo, *ACS Energy Lett.* **3**, 46 (2017).
- ¹⁴F. Gu, S. Ye, Z. Zhao, H. Rao, Z. Liu, Z. Bian, and C. Huang, *Sol. RRL* **2**, 1800136 (2018).
- ¹⁵Y. Liao, H. Liu, W. Zhou, D. Yang, Y. Shang, Z. Shi, B. Li, X. Jiang, L. Zhang, L. N. Quan, R. Quintero-Bermudez, B. R. Sutherland, Q. Mi, E. H. Sargent, and Z. Ning, *J. Am. Chem. Soc.* **139**, 6693 (2017).
- ¹⁶S. Shao, J. Liu, G. Portale, H.-H. Fang, G. R. Blake, G. H. ten Brink, L. J. A. Koster, and M. A. Loi, *Adv. Energy Mater.* **8**, 1702019 (2017).
- ¹⁷K. Chen, P. Wu, W. Yang, R. Su, D. Luo, X. Yang, Y. Tu, R. Zhu, and Q. Gong, *Nano Energy* **49**, 411 (2018).
- ¹⁸C. Ran, J. Xi, W. Gao, F. Yuan, T. Lei, B. Jiao, X. Hou, and Z. Wu, *ACS Energy Lett.* **3**, 713 (2018).
- ¹⁹G. Grancini, C. Roldán-Carmona, I. Zimmermann, E. Mosconi, X. Lee, D. Martineau, S. Narbey, F. Oswald, F. de Angelis, M. Grätzel, and M. K. Nazeeruddin, *Nat. Commun.* **8**, 15684 (2017).
- ²⁰D. S. Lee, J. S. Yun, J. Kim, A. M. Soufiani, S. Chen, Y. Cho, X. Deng, J. Seidel, S. Lim, S. Huang, and A. W. Y. Ho-Baillie, *ACS Energy Lett.* **3**, 647 (2018).
- ²¹C. C. Stoumpos, C. M. M. Soe, H. Tsai, W. Nie, J.-C. Blancon, D. H. Cao, F. Liu, B. Traoré, C. Katan, J. Even, A. D. Mohite, and M. G. Kanatzidis, *Chem* **2**, 427 (2017).
- ²²C. Keil and D. Schlettwein, *Org. Electron.* **12**, 1376 (2011).
- ²³C. C. Stoumpos, C. D. Malliakas, and M. G. Kanatzidis, *Inorg. Chem.* **52**, 9019 (2013).
- ²⁴T. Lenzer, S. Schubert, F. Ehlers, P. W. Lohse, M. Scholz, and K. Oum, *Arch. Biochem. Biophys.* **483**, 213 (2009).
- ²⁵A. L. Dobryakov, S. A. Kovalenko, A. Weigel, J. L. Pérez-Lustres, J. Lange, A. Müller, and N. P. Ernsting, *Rev. Sci. Instrum.* **81**, 113106 (2010).
- ²⁶K. Oum, O. Flender, P. W. Lohse, M. Scholz, A. Hagfeldt, G. Boschloo, and T. Lenzer, *Phys. Chem. Chem. Phys.* **16**, 8019 (2014).
- ²⁷M. Stumpp, R. Ruess, J. Horn, J. Tinz, and D. Schlettwein, *Phys. Status Solidi A* **213**, 38 (2016).
- ²⁸M. Stumpp, R. Ruess, J. Müßener, and D. Schlettwein, *Mater. Today Chem.* **4**, 97 (2017).
- ²⁹H. J. Snaith, A. Abate, J. M. Ball, G. E. Eperon, T. Leijtens, N. K. Noel, S. D. Stranks, J. T.-W. Wang, K. Wojciechowski, and W. Zhang, *J. Phys. Chem. Lett.* **5**, 1511 (2014).
- ³⁰W. Tress, N. Marinova, T. Moehl, S. M. Zakeeruddin, M. K. Nazeeruddin, and M. Grätzel, *Energy Environ. Sci.* **8**, 995 (2015).
- ³¹B. Chen, M. Yang, S. Priya, and K. Zhu, *J. Phys. Chem. Lett.* **7**, 905 (2016).
- ³²Z. Xiao, Y. Yuan, Y. Shao, Q. Wang, Q. Dong, C. Bi, P. Sharma, A. Gruverman, and J. Huang, *Nat. Mater.* **14**, 193 (2015).
- ³³S. Meloni, T. Moehl, W. Tress, M. Frankevičius, M. Saliba, Y. H. Lee, P. Gao, M. K. Nazeeruddin, S. M. Zakeeruddin, U. Rothlisberger, and M. Grätzel, *Nat. Commun.* **7**, 10334 (2016).
- ³⁴D.-Y. Son, S.-G. Kim, J.-Y. Seo, S.-H. Lee, H. Shin, D. Lee, and N.-G. Park, *J. Am. Chem. Soc.* **140**, 1358 (2018).
- ³⁵O. Almora, C. Aranda, I. Zarazua, A. Guerrero, and G. Garcia-Belmonte, *ACS Energy Lett.* **1**, 209 (2016).
- ³⁶T. Noma, D. Taguchi, T. Manaka, and M. Iwamoto, *J. Appl. Phys.* **124**, 175501 (2018).
- ³⁷J. M. Azpiroz, E. Mosconi, J. Bisquert, and F. de Angelis, *Energy Environ. Sci.* **8**, 2118 (2015).
- ³⁸T. Shi, H.-S. Zhang, W. Meng, Q. Teng, M. Liu, X. Yang, Y. Yan, H.-L. Yip, and Y.-J. Zhao, *J. Mater. Chem. A* **5**, 15124 (2017).
- ³⁹L. Pedesseau, D. Saporì, B. Traore, R. Robles, H.-H. Fang, M. A. Loi, H. Tsai, W. Nie, J.-C. Blancon, A. Neukirch, S. Tretiak, A. D. Mohite, C. Katan, J. Even, and M. Kepenekian, *ACS Nano* **10**, 9776 (2016).
- ⁴⁰K. Ghimire, D. Zhao, Y. Yan, and N. J. Podraza, *AIP Adv.* **7**, 075108 (2017).
- ⁴¹O. Flender, J. R. Klein, T. Lenzer, and K. Oum, *Phys. Chem. Chem. Phys.* **17**, 19238 (2015).
- ⁴²J. R. Klein, O. Flender, M. Scholz, K. Oum, and T. Lenzer, *Phys. Chem. Chem. Phys.* **18**, 10800 (2016).
- ⁴³J. Yang, X. Wen, H. Xia, R. Sheng, Q. Ma, J. Kim, P. Tapping, T. Harada, T. W. Kee, F. Huang, Y.-B. Cheng, M. Green, A. Ho-Baillie, S. Huang, S. Shrestha, R. Patterson, and G. Conibeer, *Nat. Commun.* **8**, 14120 (2017).
- ⁴⁴M. B. Johnston and L. M. Herz, *Acc. Chem. Res.* **49**, 146 (2016).
- ⁴⁵L. Ma, F. Hao, C. C. Stoumpos, B. T. Phelan, M. R. Wasielewski, and M. G. Kanatzidis, *J. Am. Chem. Soc.* **138**, 14750 (2016).